



This is a repository copy of *Design, analysis and experimental evaluation of a novel high-speed high-power ferrite IPM machine for traction applications*.

White Rose Research Online URL for this paper:

<https://eprints.whiterose.ac.uk/192512/>

Version: Accepted Version

---

**Proceedings Paper:**

Hoang, K.D. orcid.org/0000-0001-7463-9681, Yu, A., Ullah, S. et al. (3 more authors) (2022) Design, analysis and experimental evaluation of a novel high-speed high-power ferrite IPM machine for traction applications. In: IEEE energy conversion congress and expo (ECCE) 2022. IEEE energy conversion congress and expo (ECCE 2022), 09-13 Oct 2022, Detroit, Michigan, USA. Institute of Electrical and Electronics Engineers (IEEE) , pp. 1-7. ISBN 9781728193885

<https://doi.org/10.1109/ECCE50734.2022.9947551>

---

© 2022 IEEE. Personal use of this material is permitted. Permission from IEEE must be obtained for all other users, including reprinting/ republishing this material for advertising or promotional purposes, creating new collective works for resale or redistribution to servers or lists, or reuse of any copyrighted components of this work in other works. Reproduced in accordance with the publisher's self-archiving policy.

**Reuse**

Items deposited in White Rose Research Online are protected by copyright, with all rights reserved unless indicated otherwise. They may be downloaded and/or printed for private study, or other acts as permitted by national copyright laws. The publisher or other rights holders may allow further reproduction and re-use of the full text version. This is indicated by the licence information on the White Rose Research Online record for the item.

**Takedown**

If you consider content in White Rose Research Online to be in breach of UK law, please notify us by emailing [eprints@whiterose.ac.uk](mailto:eprints@whiterose.ac.uk) including the URL of the record and the reason for the withdrawal request.



[eprints@whiterose.ac.uk](mailto:eprints@whiterose.ac.uk)  
<https://eprints.whiterose.ac.uk/>

# Design, Analysis and Experimental Evaluation of a Novel High-Speed High-Power Ferrite IPM Machine for Traction Applications

Khoa Dang Hoang  
*Dept. of Engineering and Technology*  
*University of Huddersfield*  
Huddersfield, United Kingdom  
d.k.hoang@hud.ac.uk

Anshan Yu  
*Senior Engineer*  
*Altair China*  
China  
anshanyu@altair.com

Sana Ullah  
*School of Engineering*  
*Newcastle University*  
Newcastle upon Tyne, United Kingdom  
sana.ullah@newcastle.ac.uk

Kais Atallah  
*Dept. of Electronic and Electrical*  
*Engineering*  
*University of Sheffield*  
Sheffield, United Kingdom  
k.atallah@sheffield.ac.uk

Giorgio Valente  
*Manufacturing Intelligence Division*  
*Hexagon*  
Nottingham, United Kingdom  
giorgio.valente@hexagon.com

Annabel Shahaj  
*Manufacturing Intelligence Division*  
*Hexagon*  
Nottingham, United Kingdom  
annabel.shahaj@hexagon.com

**Abstract**—The paper presents the design and experimental evaluation of a novel (12000rpm, 80kW) Ferrite IPM machine for traction applications. First, the Ferrite IPM machine concept employing both circumferential and axial permanent magnets for airgap flux density improvement is introduced. An extensive sizing exercise to maximize the axial magnet contribution and meet the required torque-speed characteristic within the specified space envelope is undertaken, which led to the selection of a multi-stack rotor concept. In order to avoid the computationally intensive 3D FEA, an equivalent 2D FEA model is developed and employed for the design optimization of the traction machine. A full-size prototype Ferrite IPM traction machine is developed and tested, and it is shown that a maximum efficiency of 97% can be achieved.

**Keywords**—Axial magnet, efficiency, driving cycle, FERRITE magnet, interior permanent magnet (IPM) machine, spoke-type IPM machine, traction machine.

## I. INTRODUCTION

IPM machines with rare-earth permanent magnets (PMs) are often employed for traction applications due to their high torque density, high efficiency, as well as good field weakening operation ability [1], [2]. However, rare-earth PMs are expensive and prone to significant price fluctuations and supply-chain uncertainties [3]. Therefore, rare-earth free traction machine topologies such as zero-magnet machines including induction machines (IM), switched reluctance machine (SRM), synchronous reluctance machine (SynRM) [4]-[10] or ferrite magnet machine providing comparable performances have been the subject of significant interest from academia and industry [11]-[18].

In [4], optimal design of an IM was presented where a measured efficiency up to 95% could be achieved. An IM design technique for energy-saving operation over wide frequency range was introduced in [5]. Design and development of an SRM for hybrid electric vehicles with a maximum 95% efficiency is reported in [6]. The effect of stator/rotor segments on SRM performance was investigated in [7]. In [8], a comparative study between IPM machine and non-rare-earth machines such as IM and SRM is introduced. Optimum design of SynRM with multi-objective optimization was introduced in [9] where a maximum efficiency as 91% was obtained. In addition, dual-phase material was proposed

for SynRM to reduce the leakage effects on machine performance resulting in 95% maximum efficiency and 5:1 constant power speed ratio [10].

Replacement of rare-earth PMs by low-cost rare-earth free PMs such as ferrite magnets is also another subject of interest [11]-[18]. Design of a ferrite-assisted SynRM machine considering demagnetization risks under low temperature was presented in [11] and [12]. In addition, a two-segment spoke type ferrite IPM machine concept with better performance and demagnetization protection was proposed in [13]. Measured efficiency up to 95% for a ferrite spoke type IPM machine under full load condition was reported in [14]. In addition, 2D and 3D demagnetization study of a ferrite IPM traction machine was respectively reported in [15] and [16] where it is shown that a reduction of stack length may mitigate the demagnetization risk due to the relevant increase of stator reluctance. To reduce leakage flux and improve torque density, two type rotor cores with and without rotor bridges was combined together for a ferrite spoke type IPM machine [17]. A comprehensive study on opportunities and challenges of rare-earth free alternatives was presented in [18]. It is noted that due to its low remanence flux density, airgap flux density of ferrite IPM machines are significantly lower than rare-earth IPM machines.

For airgap flux density improvement, a novel ferrite IPM machine concept employing a unique configuration of circumferential and axial ferrite PM with an achievable airgap flux density higher than 1T was proposed in [19] and experimentally validated in [20]. To maximize the airgap flux density, the ratio of the axial length to the rotor diameter should be minimized, Fig. 1. In the paper, the concept will be further investigated to meet the requirements of a traction application, and the performance of the ferrite IPM and a benchmark rare-earth IPM are compared [21].

Therefore, the paper presents the design and experimental evaluation of a ferrite IPM machine (12000rpm, 80kW) for traction applications. It is shown that airgap flux density of the proposed concept can be significantly improved using axial permanent magnets. It is also demonstrated that a maximum efficiency of 97% can be achieved.

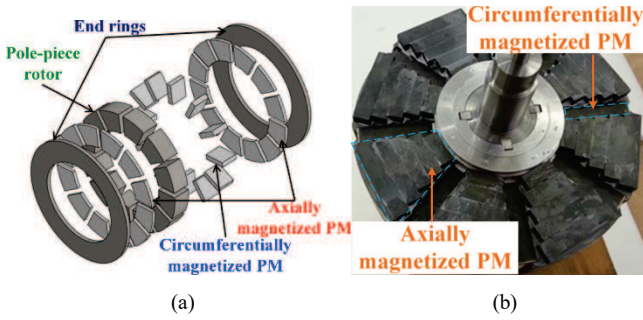


Fig. 1. Ferrite-based IPM machine concept with axially magnetized PM [19], [20]. (a) Machine topology. (b) Prototype rotor with axial and circumferential PMs.

TABLE I - FERRITE MACHINE DESIGN SPECIFICATIONS

Peak/continuous torque (Nm)	245/120
Base/maximum speed (rpm)	3750/12000
Peak current (A)	290
DC-link voltage (V)	600

## II. FERRITE CONCEPT DEVELOPMENT FOR TRACTION APPLICATION

In the section, design development of the ferrite machine concept in [19] and [20] to meet the requirement of a traction application, Table I, is presented. The benchmark rare-earth IPM machine (BM) parameters including space envelope is provided in Table II and a cross-sectional view is shown Fig. 6(e).

### A. Sizing of ferrite IPM machine

Initially, the machine sizing is determined. Starting from a spoke-type IPM rotor for a high airgap flux density, Fig. 1, several configurations are investigated. First, the effects of the combinations of pole pairs and split-ratios between the stator bore diameter (ID) and outer diameter (OD) on normalized torque density TD (Torque/Volume/Constant) [22] are shown in Fig. 2(a). As can be seen, for the number of pole pairs from 3 to 6, the split-ratio should be between 0.5 and 0.7. With a maximum operation speed of 12000rpm, Table I, it is essential that the number of pole pairs is chosen in such a way that the fundamental frequency is controllable by a traction inverter. On the other hand, using the lumped parameter circuit [19], and FEA, and for a fixed rotor diameter, circumferential and axial ferrite magnet thicknesses, the effects of the active length on the airgap flux density is depicted in Fig. 2(b). As can be seen, to maximize the axial ferrite PMs contribution to the airgap flux density, the ratio of axial length to rotor diameter (named as rotor aspect ratio) should be minimized.

The results in Fig. 2 are utilized for an extensive analytical parameter scanning to determine the optimum initial size of the ferrite IPM machine, which meets the specification requirements within the specified spatial constraints. The effects of pole pair number, rotor ID, rotor OD, rotor aspect ratio, circumferential magnet thickness, axial magnet thickness, bolt diameter, split-ratio, on torque density are shown in Fig. 3. It can be seen that a single-stack with a low aspect ratio result in the highest torque densities. However, this would require a stator OD larger than the specified stator OD of 180mm. Therefore, to maintain the rotor aspect ratio and maximize the axial PM contribution while satisfying the available space envelope, a multi-stack rotor topology should be adopted.

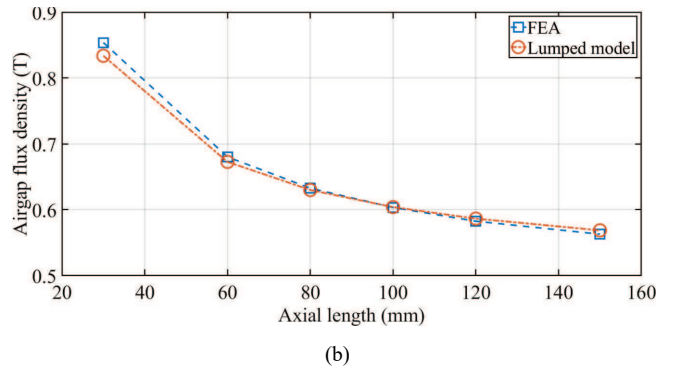
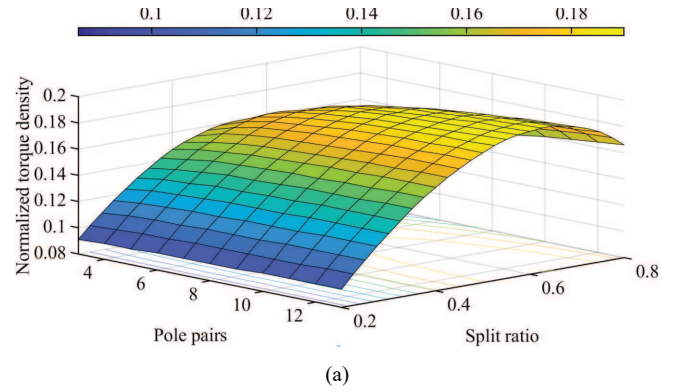


Fig. 2. Initial sizing step for ferrite machine. (a) Optimum pole-pairs and split-ratio for maximizing torque density [22]. (b) Average airgap flux density vs axial length with fixed circumferential and axial ferrite magnet thickness [19].

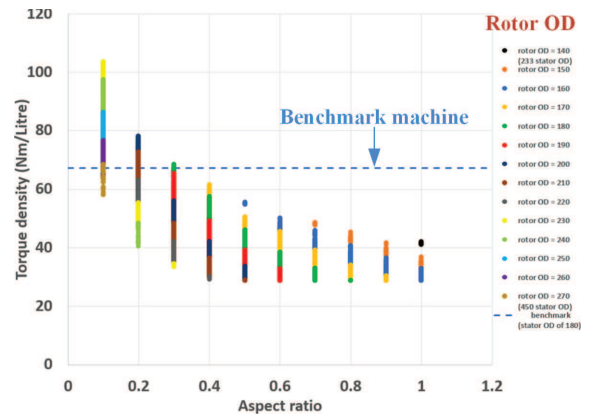


Fig. 3. Determination of machine sizing via extensive analysis targeting for a given torque density.

TABLE II – INTENSIVE SIZING DEVELOPMENT

Design no.	1554	260671	4604083	<b>5610296</b>	5605943	BM
Stack no.	2	3	3	3	4	<b>1</b>
Slot/pole	48/8	60/10	60/10	60/10	60/10	<b>48/8</b>
J (Arms/mm <sup>2</sup> )	31	28	28	28	28	<b>28</b>
Active axial length (mm)	166	160	166	189	192	<b>155</b>
Total axial length (mm)	234	250	238	255	272	<b>232</b>
Fundamental airgap flux density (T)	0.9	1.02	0.9	0.9	0.9	<b>0.9</b>
Rotor OD (mm)	126	126	126	126	126	<b>126</b>
Rotor ID (mm)	40	42	55	65	65	<b>55</b>
<b>Stator OD (mm)</b>	<b>180</b>	<b>180</b>	<b>180</b>	<b>180</b>	<b>180</b>	<b>180</b>
Peak Torque (Nm)	237	236	234	257	251	<b>240</b>

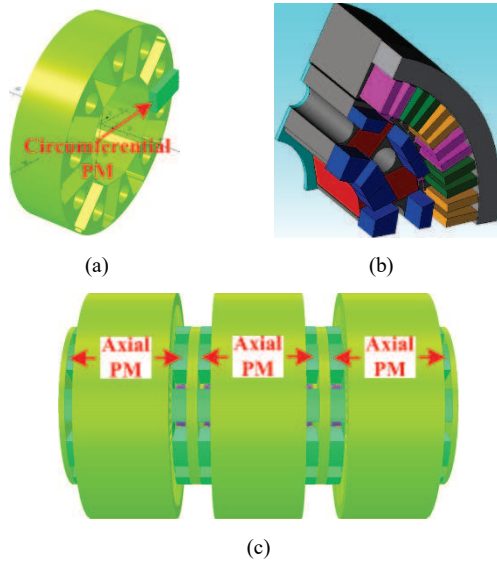


Fig. 4. Optimum rotor sizing. (a) Rotor stack with circumferential PM. (b) One-half stack 3D model. (c) Final rotor sizing with 3 separated stacks.

Table II presents feasible concepts from the analytical sizing procedure, taking into consideration of the fixed stator OD of 180mm. The benchmark rare-earth IPM machine has also been included in the table for a comparison and highlighted in blue. It may be noted that these designs are down selected from more than 5 million designs generated by the analytical study. As could be seen in Table II, each specific sizing concept is associated with a number. It is noted that the ferrite machine is designed for traction application with half-shaft connection. Therefore, rotor ID parameter is also highly essential for maintaining gearbox connection.

### B. Design optimization of ferrite IPM machine

Based on the sizing envelop limitation, the mechanical connection requirement (high rotor ID for half-shaft connection), and the torque-speed performance, the design number 5610296 with 3-stack topology is selected for the design optimization, Fig. 4. For design analysis, the M235-35A magnetic steel [23] is utilized for stator and rotor core while the TDK FB9H [24] is employed for the rotor ferrite magnet. As can be seen,  $BH$ -curve of the selected ferrite magnet is very linear down to  $-60$  degrees Celsius, Fig. 5. The characteristics of the employed ferrite at 20 Celsius degrees and  $-10$  Celsius degrees extracted from Fig. 5 is presented in Table III.

#### 1) Stator design

Since the spoke-type rotor is well-known for high spatial harmonics [25], a distributed winding with shorted-pitch (5/6) is selected to minimize winding harmonics. For reduction of AC losses, multi-strand conductor is employed. FEA and measurement on the machine prototype (Fig. 10) show that at maximum operation speed (12000rpm), an increase up to 130% of stator resistance at 20 Celsius degrees could be observed. In addition, the tooth width and the back-iron thickness are selected to minimize the torque ripple. The winding turn-number and conductor area is defined based on the torque-speed characteristic, DC-link voltage, cooling methodology, and the achieved slot-filling factor. The machine winding insulation is class H. The machine casing is equipped with water-jacket cooling and the flow-rate is as 6.5 liters/minute. The machine airgap is selected as high as 0.75mm for easing of manufacturing and safety performance regarding long axial rotor shaft, Table II.

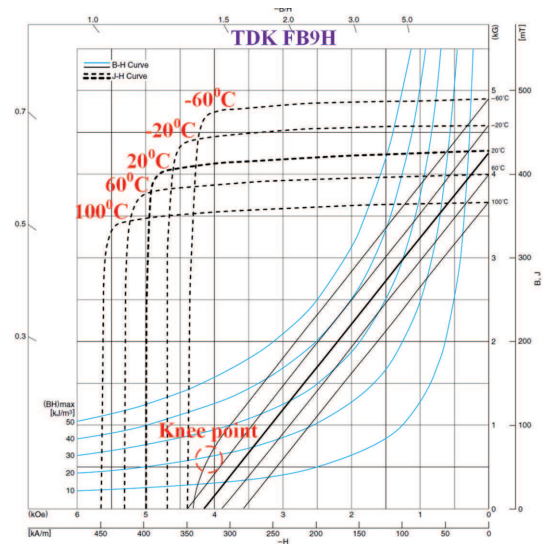


Fig. 5.  $BH$ -curve of employed ferrite magnet (TDK-FB9H) [24].

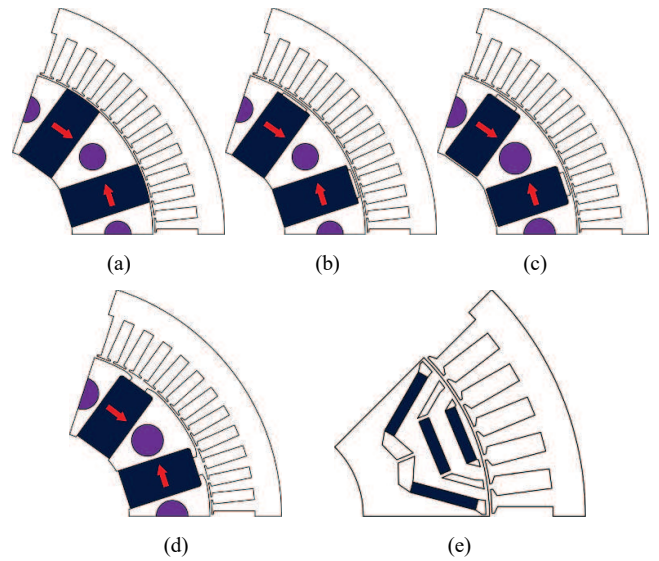


Fig. 6. Evolution of rotor design. (a) Initial design. (b) Close-bridge rotor, low torque ripple. (c) Close-bridge rotor, high active length. (d) Open-bridge rotor, final concept. (e) Benchmark rare-earth machine.

TABLE III FB9H FERRITE CHARACTERISTICS AT 20 AND  $-10$  CELSIUS DEGREES [24]

Temp.	$B_r$ (T)	$H_c$ (kA/m)	$H_{ci}$ (kA/m)	$H_c$ knee (kA/m)
$20^\circ\text{C}$	0.43	330.2	397.9	378
$-10^\circ\text{C}$	0.445	350	364	347

#### 2) Rotor design

Based on the initial rotor concept, Fig. 6(a), and for a given axial length, the circumferential and axial magnet thicknesses are selected to maximize the airgap flux density and avoid demagnetization. For the ferrite IPM machine, the magnet thickness should be determined so that it can sustain transient short-circuit current at the minimum temperature of  $-10$  degrees Celsius without risk of irreversible demagnetization, Fig. 5. Then, in the 2<sup>nd</sup> rotor concept, the outer bridge is introduced for the magnet retention, Fig. 6(b). Fig. 6(c) illustrates the 3<sup>rd</sup> concept with bigger bolt diameter, wider outer bridge thickness and introduction of the inner bridge for better sustainable structural performance. However, rotor bridges result in leakage flux leading to reduction in airgap flux density. Selected final configuration is illustrated in Fig. 6(d) with open bridges to reduce the leakage flux and

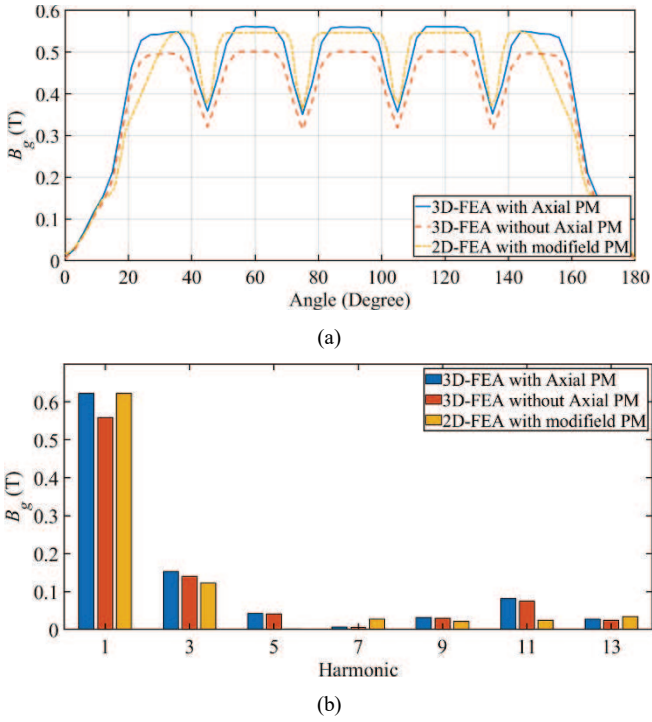


Fig. 7. Airgap flux density of ferrite concept. (a) Airgap flux waveform. (b) Harmonic spectrum.

maximize the airgap flux density. However, an open bridge may result in a higher demagnetization risk for the top magnet area due to the concentration of leakage flux-line over this region [15] (see section IV). For illustration purpose, the benchmark rotor is also depicted in Fig. 6(e). The rotor design optimization evolved from the 1<sup>st</sup> concept to the final concept due to mechanical considerations under maximum speed operation and efficiency over WLTP driving cycle. It is worth noting that both the ferrite machine and the benchmark rare-earth machine are with similar outer diameter as shown in Table II.

### III. EVALUATION OF PROPOSED TOPOLOGY WITH 3D FEA MODEL AND EQUIVALENT 2D FEA MODEL

To investigate the performance of the proposed topology with axial PMs, 3D FEA is utilized and no-load airgap flux density with and without axial PMs is shown in Fig. 7. As can be seen, for the proposed topology, an increase of 13% in fundamental airgap flux density could be achieved by adding the axial PMs. However, in order to simplify the analysis, an equivalent 2D FEA model, where only the circumferential PMs are considered is adopted. In order to take into account of the contribution from the axial PMs, the magnetic properties of the circumferential PMs are modified using the lumped parameter model [19] to achieve the same fundamental airgap flux density Fig. 7.

### IV. DEMAGNETIZING INVESTIGATION

In comparison with rare-earth magnet, ferrite magnet coercivity,  $H_{ci}$ , is around one-third in value [15]. For traction application, high  $d$ -axis current under peak torque demand is often required. In addition, under transient shorted-circuit fault, a transient peak current with significantly higher value than the rated current could be occurred, Figs. 8(a) and 8(b). Therefore, the evaluation of the risk demagnetization risk is essential. As the  $BH$  curve of the employed magnet (FB9H) in the 2<sup>nd</sup> quadrant is very linear except under -60 Celsius degrees, Fig. 5, the field strength for demagnetization analysis

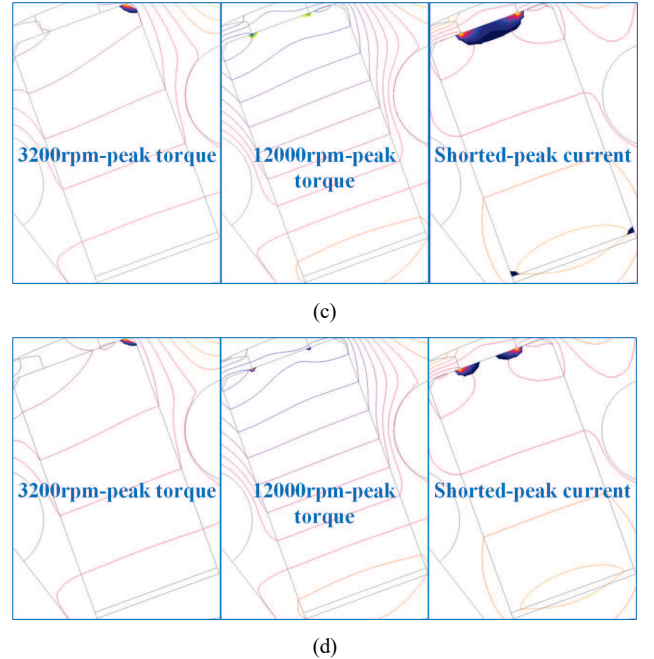
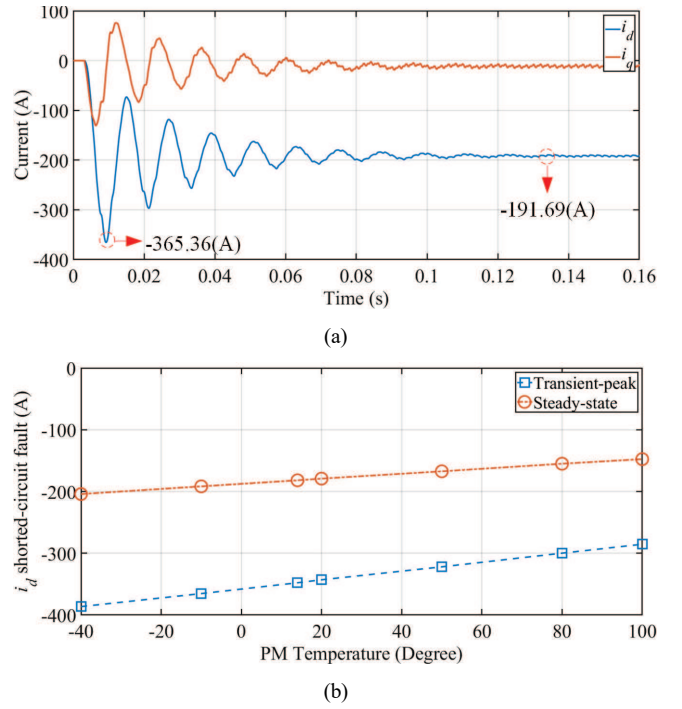


Fig. 8. Demagnetization analysis. (a) Transient shorted-circuit fault at -10 Celsius degree. (b)  $D$ -axis transient and steady-state shorted-circuit current under different PM temperatures. (c) Field strength contour for higher level than 95% of intrinsic coercivity, -10 Celsius-degree PM. (d) Field strength contour for higher level than 95% of intrinsic coercivity, 20 Celsius-degree PM.

for each temperature value is defined as a 95% of its intrinsic coercive force ( $H_{ci}$ ), Table III. During the design optimization step (see section II), several measures for demagnetization protection have been considered. Such measures include adjusting of the circumferential and axial magnet thicknesses to increase magnet reluctance in relevant axis.

Field strength contour with higher level than 95% of relevant intrinsic coercive force ( $H_{ci}$ ), Table III, for the ferrite machine under normal operation condition and shorted-circuit fault condition (peak current) with -10 Celsius-degree PM and 20 Celsius-degree PM is respectively presented in Fig. 8(c) and 8(d). As can be seen, in normal operation condition for

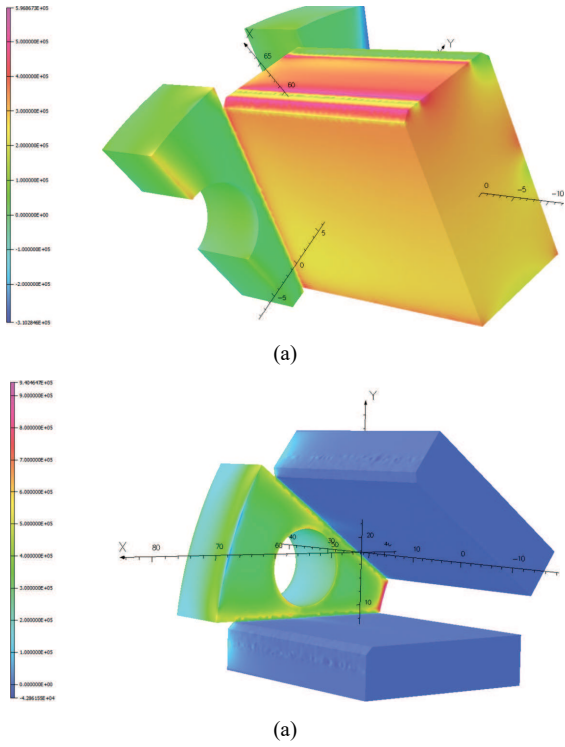


Fig. 9. 3D FEA demagnetization analysis for -10 Celsius degree PM. (a) Circumferential magnet. (b) Axial magnet.

both -10 Celsius-degree and 20 Celsius-degree PM, the magnet area under demagnetizing risk is very limited (only less than 1%). This demonstrates the performance capability of the ferrite machine under low-temperature conditions.

On the other hand, in shorted-circuit fault condition, around 4.2% magnet area with -10 Celsius-degree and 1.8% magnet area with 20 Celsius-degree exhibit a high risk of demagnetization, Figs. 8(c) and 8(d). This could not mitigate by adjusting the magnet thicknesses. It is also noted that the demagnetizing area is significantly small (5%) and the direction is mainly in radial axis which may not significantly affect to the ferrite machine performance. However, to strengthen the rotor structure and mitigate the demagnetization risk under low temperature, a 0.4mm thick spacer is inserted between the bridge and the magnet [26].

The shorted currents in 2D FEA are also applied to 3D FEA for further demagnetization investigation. By way of example, Fig. 9 shows 3D FEA study with the transient shorted-circuit currents for -10 Celsius degree PM, Fig. 8(a). As can be seen, the circumferential magnet shows 4.92% area under demagnetization risk while the axial magnet depicts 7.68% area with demagnetization risk.

## V. EXPERIMENTAL VALIDATION OF PROPOSED CONCEPT

A prototype ferrite IPM machine (1200rpm, 80kW) is built to validate the predictions and demonstrate the performance of the proposed topology, Fig. 10. During testing, the prototype is controlled under torque control mode while the dyno is controlled under speed control mode, Fig. 10(c).

Fig. 11 compares measured and predicted, using 2D FEA, back-EMF waveform and its harmonic spectrum. It can be seen that a very good agreement exists, which demonstrates the effectiveness of the proposed 2D FEA model. On the other hand, measurement validation of the machine performance via torque and flux linkage maps is illustrated in Fig. 12 where a

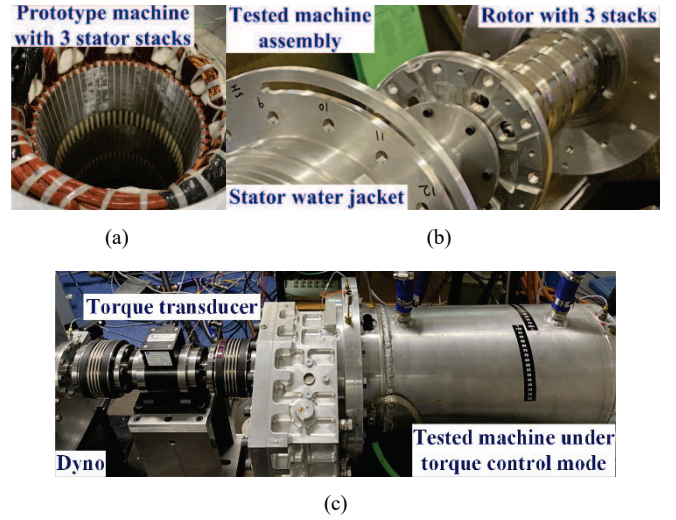


Fig. 10. Prototype ferrite IPM machine. (a) Stator. (b) Rotor. (c) Test-rig.

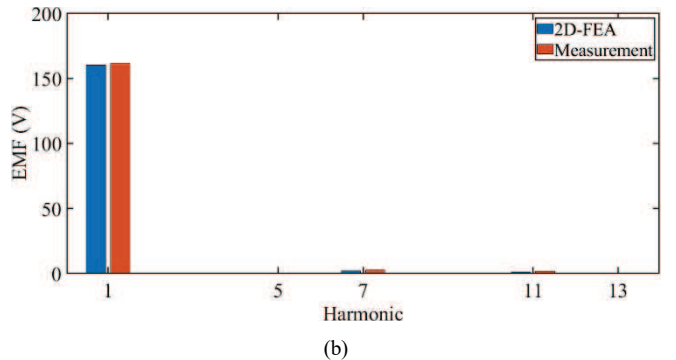
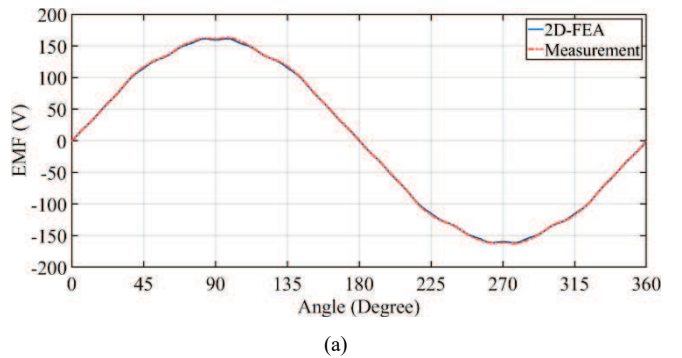


Fig. 11. Line-line back-EMF at 1288rpm. (a) Waveform. (b). Harmonic spectrum.

maximum of 4% differences between measurement and 2D FEA could be observed. The measured torque and flux linkage maps, are used to produce  $dq$ -axis current references over torque speed curve [1]. For control development, the machine is under maximum torque per ampere (MTPA) control in the low-speed region and field-weakening (FW) control in the high-speed region [1].

Figs. 13 (a) and (b) show the predicted efficiency maps of the proposed and the benchmark machines, respectively. It can be seen that efficiencies as high as those for the benchmark machine can be achieved. Furthermore, for the ferrite machine, good agreement between measured and predicted using 2D FEA, efficiencies under 3000rpm and 10000rpm operation conditions, can be observed in Figs. 14(a), and (b), respectively. In addition, good agreement between 2D FEA with modified PM, 3D FEA, and measured torque under MTPA operation at 1500rpm is shown in Fig. 14(c).

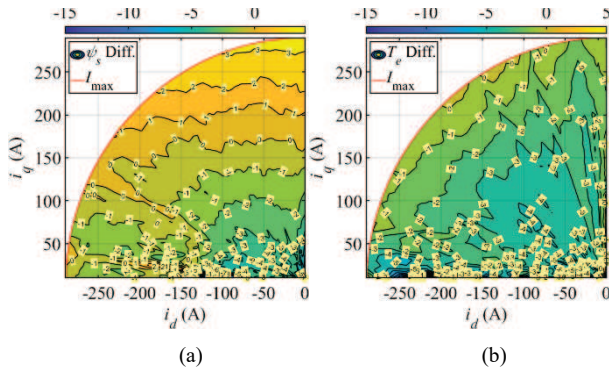


Fig. 12. Difference between measurement and 2D FEA. (a) Stator flux linkage map. (b) Torque map.

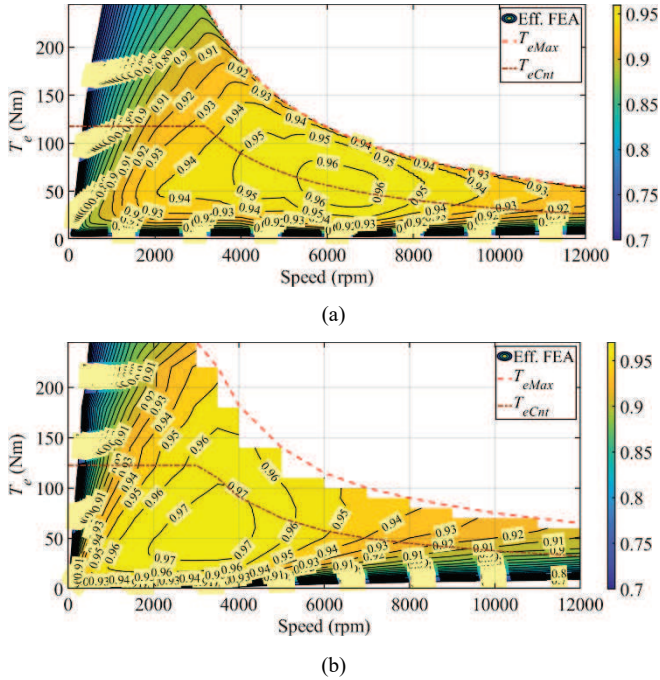


Fig. 13. Analytical efficiency map. (a) Ferrite machine. (b) Benchmark rare-earth machine.

## VI. CONCLUSIONS

The paper presents the design and experimental evaluation of a novel ferrite IPM machine topology for traction applications. It is shown that adding axial PMs enhances the airgap flux density. It is also shown that efficiencies similar to equivalent rare-earth IPM machine can be achieved. Furthermore, despite the 3D nature of the magnetic field distribution in the rotor, it shown that an equivalent 2D FEA model can provide accurate predictions of the key performance indicators. The proposed concept is highly demonstrated via measurements on the 80kW prototype machine with up to 97% efficiency achievement.

## ACKNOWLEDGMENT

The work was undertaken at the University of Sheffield, UK in collaboration with Hexagon and was supported by Innovate UK, under the EDISON project.

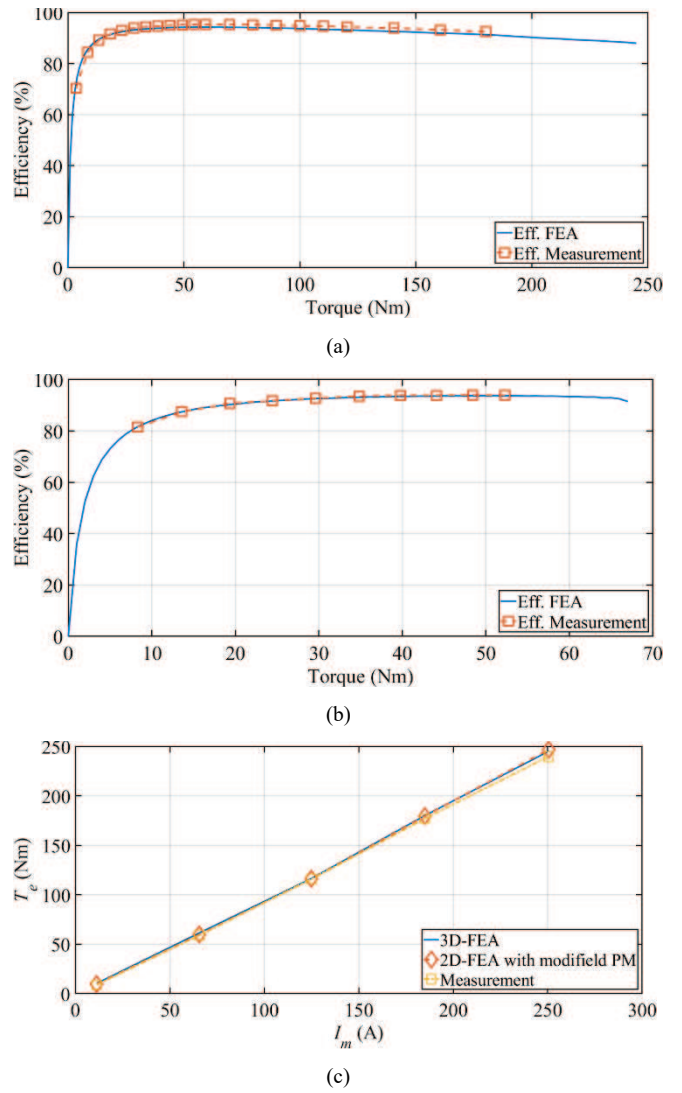


Fig. 14. Ferrite machine validation. (a) Measured and calculated efficiency at 3000rpm. (b) Measured and calculated efficiency at 10000rpm. (c). Measured and calculated torque under MTPA operation at 1500rpm.

## REFERENCES

- [1] K. D. Hoang, P. Lazari, K. Atallah, J. G. Birchall and S. D. Calverley, "Evaluation of simplified model for rapid identification and control development of IPM traction machines," in *IEEE Trans. Transportation Electrification*, vol. 7, no. 2, pp. 779-792, June 2021.
- [2] K. D. Hoang, "Simplified analytical model for rapid evaluation of interior PM traction machines considering magnetic nonlinearity," in *IEEE Open Journal of the Industrial Electronics Society*, vol. 1, pp. 340-354, 2020.
- [3] Nabeel A. Mancheri, Benjamin Sprecher, Gwendolyn Bailey, Jianping Ge, Arnold Tukker, "Effect of Chinese policies on rare earth supply chain resilience", *Resources, Conservation and Recycling*, vol. 142, 2019, pp. 101-112.
- [4] T. -V. Tran, E. Nègre, K. Mikati, P. Pellerey and B. Assaad, "Optimal design of TEFC induction machine and experimental prototype testing for city battery electric vehicle," in *IEEE Tran. Industry Applications*, vol. 56, no. 1, pp. 635-643, Jan.-Feb. 2020.
- [5] M. Dems and K. Komez, "Designing an energy-saving induction motor operating in a wide frequency range," in *IEEE Transactions on Industrial Electronics*, vol. 69, no. 5, pp. 4387-4397, May 2022.
- [6] M. Takeno, A. Chiba, N. Hoshi, S. Ogasawara, M. Takemoto and M. A. Rahman, "Test results and torque improvement of the 50-kW switched reluctance motor designed for hybrid electric vehicles," in *IEEE Trans. Industry Applications*, vol. 48, no. 4, pp. 1327-1334, July-Aug. 2012.

- [7] V. R. and B. G. Fernandes, "Design methodology for high-performance segmented rotor switched reluctance motors," in *IEEE Trans. Energy Conversion*, vol. 30, no. 1, pp. 11-21, March 2015.
- [8] Z. Yang, F. Shang, I. P. Brown and M. Krishnamurthy, "Comparative study of interior permanent magnet, induction, and switched reluctance motor drives for EV and HEV applications," in *IEEE Trans. Transportation Electrification*, vol. 1, no. 3, pp. 245-254, Oct. 2015.
- [9] F. Cupertino, G. Pellegrino and C. Gerada, "Design of synchronous reluctance motors with multiobjective optimization algorithms," in *IEEE Trans. Industry Applications*, vol. 50, no. 6, pp. 3617-3627, Nov.-Dec. 2014.
- [10] P. B. Reddy, A. M. El-Refaie, S. Galioto and J. P. Alexander, "Design of synchronous reluctance motor utilizing dual-phase material for traction applications," in *IEEE Trans. Industry Applications*, vol. 53, no. 3, pp. 1948-1957, May-June 2017.
- [11] A. Vagati, B. Boazzo, P. Guglielmi and G. Pellegrino, "Design of ferrite-assisted synchronous reluctance machines robust toward demagnetization," in *IEEE Trans. Industry Applications*, vol. 50, no. 3, pp. 1768-1779, May-June 2014.
- [12] D. G. Dorrell, M. Hsieh and A. M. Knight, "Alternative rotor designs for high performance brushless permanent magnet machines for hybrid electric vehicles," in *IEEE Trans. Magnetics*, vol. 48, no. 2, pp. 835-838, Feb. 2012.
- [13] S. Kim, J. Cho, S. Park, T. Park and S. Lim, "Characteristics comparison of a conventional and modified spoke-type ferrite magnet motor for traction drives of low-speed electric vehicles," in *IEEE Trans. Industry Applications*, vol. 49, no. 6, pp. 2516-2523, Nov.-Dec. 2013.
- [14] S. J. Galioto, P. B. Reddy, A. M. EL-Refaie and J. P. Alexander, "Effect of magnet types on performance of high-speed spoke interior-permanent-magnet machines designed for traction applications," in *IEEE Trans. Industry Applications*, vol. 51, no. 3, pp. 2148-2160, May-June 2015.
- [15] M. Kimiabeigi *et al.*, "High-performance low-cost electric motor for electric vehicles using ferrite magnets," in *IEEE Trans. Industrial Electronics*, vol. 63, no. 1, pp. 113-122, Jan. 2016.
- [16] M. Kimiabeigi, J. D. Widmer, N. J. Baker, R. Martin, B. C. Mecrow and A. Michaelides, "Three-dimensional modelling of demagnetization and utilization of poorer magnet materials for EV/HEV applications," in *IEEE Trans. Energy Conversion*, vol. 31, no. 3, pp. 981-992, Sept. 2016.
- [17] J. -W. Jung, K. -T. Jung, B. -H. Lee and J. -P. Hong, "Design and analysis of ferrite magnet flux concentrated PMSM with cross-laminated rotor core using equivalent 2-D FEA," in *IEEE Trans. Energy Conversion*, vol. 34, no. 3, pp. 1623-1631, Sept. 2019.
- [18] H. Tahanian, M. Aliahmadi and J. Faiz, "Ferrite permanent magnets in electrical machines: opportunities and challenges of a non-rare-earth alternative," in *IEEE Trans. Magnetics*, vol. 56, no. 3, pp. 1-20, March 2020.
- [19] K. Atallah and J. Wang, "A rotor with axially and circumferentially magnetized permanent magnets," in *IEEE Trans. Magnetics*, vol. 48, no. 11, pp. 3230-3233, Nov. 2012.
- [20] A. Shanshal, K. Hoang and K. Atallah, "High-performance ferrite permanent magnet brushless machines," in *IEEE Trans. Magnetics*, vol. 55, no. 7, pp. 1-4, July 2019.
- [21] <https://patentscope.wipo.int/search/en/detail.jsf?docId=WO2017220430>.
- [22] L. J. Wu, Z. Q. Zhu, J. T. Chen, Z. P. Xia and G. W. Jewell, "Optimal split ratio in fractional-slot interior permanent-magnet machines with non-overlapping windings," in *IEEE Trans. Magnetics*, vol. 46, no. 5, pp. 1235-1242, May 2010.
- [23] <https://www.tatasteleurope.com/sites/default/files/m235-35a.pdf>
- [24] [https://product.tdk.com/en/search/magnet/magnet/ferrite/info?part\\_no=FB9H](https://product.tdk.com/en/search/magnet/magnet/ferrite/info?part_no=FB9H)
- [25] K. Y. Hwang, J. H. Jo and B. I. Kwon, "A study on optimal pole design of spoke-type IPMSM with concentrated winding for reducing the torque ripple by experiment design method," in *IEEE Trans. Magnetics*, vol. 45, no. 10, pp. 4712-4715, Oct. 2009.
- [26] [https://www.coolwind.co.uk/product/g10\\_fr4](https://www.coolwind.co.uk/product/g10_fr4)